Title

Multiband spectral-spatial RF excitation for hyperpolarized [2-13C]dihydroxyacetone 13C-MR metabolism studies

Journal

Magnetic Resonance in Medicine, 77(4)

ISSN

0740-3194

Authors

Marco-Rius, Irene
Cao, Peng
von Morze, Cornelius
et al.

Publication Date

2017-04-01

DOI

10.1002/mrm.26226

Peer reviewed

HHS Public Access

Author manuscript

Magn Reson Med. Author manuscript; available in PMC 2018 April 01.

Published in final edited form as:

Magn Reson Med. 2017 April ; 77(4): 1419–1428. doi:10.1002/mrm.26226.

Multiband Spectral-Spatial RF Excitation for Hyperpolarized [2-^{13}C]Dihydroxyacetone ^{13}C-MR Metabolism Studies

Irene Marco-Rius[1,5], **Peng Cao**[1], **Cornelius von Morze**[1], **Matthew Merrit**[2], **Karlos X Moreno**[3], **Gene-Yuan Chang**[4], **Michael A. Ohliger**[1], **David Pearce**[4], **John Kurhanewicz**[1], **Peder E. Z. Larson**[1], and **Daniel B. Vigneron**[1]

[1]Department of Radiology and Biomedical Imaging, University of California San Francisco, San Francisco, California

[2]Department of Biochemistry and Molecular Biology, University of Florida, Gainesville, Florida

[3]Department of Chemistry, Engineering, Pre-Pharmacy, and Physics, South Texas College, Weslaco, Texas

[4]Department of Medicine, Division of Nephrology, University of California San Francisco, San Francisco, California

Abstract

Purpose—To develop a specialized multislice, single-acquisition approach to detect the metabolites of hyperpolarized [2-^{13}C]dihydroxyacetone (DHAc) to probe gluconeogenesis in vivo, which have a broad 144 ppm spectral range (~4.6 KHz at 3T). A novel multiband RF excitation pulse was designed for independent flip angle control over 5-6 spectral-spatial (SPSP) excitation bands, each corrected for chemical shift misregistration effects.

Methods—Specialized multi-band SPSP RF pulses were designed, tested and applied to investigate hyperpolarized [2-^{13}C]DHAc metabolism in kidney and liver of fasted rats with dynamic ^{13}C-MRS and an optimal flip angle scheme. For comparison, experiments were also performed with narrow-band slice-selective RF pulses and a sequential change of the frequency offset to cover the five frequency bands of interest.

Results—The SPSP pulses provided a controllable spectral profile free of baseline distortion with improved signal to noise of the metabolite peaks, allowing for quantification of the metabolic products. We observed organ-specific differences in DHAc metabolism. There was 2-5 times more [2-^{13}C]phosphoenolpyruvate and about 19 times more [2-^{13}C]glycerol 3-phosphate in the liver than in the kidney.

Conclusion—A multiband SPSP RF pulse covering a spectral range over 144 ppm enabled in vivo characterization of HP [2-^{13}C]dihydroxyacetone metabolism in rat liver and kidney.

Keywords

spectral-spatial RF pulses; multiband RF pulses; dynamic nuclear polarization; hyperpolarization; metabolic imaging; dihydroxyacetone; kidney; liver

[5]Corresponding author: irene.marco-rius@ucsf.edu.

INTRODUCTION

Recent developments of hyperpolarization techniques, especially dissolution dynamic nuclear polarization (DNP), offer the sensitivity to monitor localized distribution and metabolism of ^{13}C-labeled substrates in vivo, providing biologically relevant information including tissue perfusion, metabolic products, and enzyme kinetics[1,2]. The most common hyperpolarized substrate for in vivo studies is [1-^{13}C]pyruvate, whose metabolic products are lactate, alanine and bicarbonate[3,4]. Recently, [2-^{13}C]dihydroxyacetone (DHAc) has emerged as a promising bio-probe for investigating gluconeogenesis[5]. Moreno et al. demonstrated that upon injection of hyperpolarized [2-^{13}C]DHAc into perfused livers, DHAc rapidly metabolized into glycerol 3-phosphate (G3P) through dihydroxyacetone phosphate (DHAP), and entered the glucose metabolic pathway at the glyceraldehyde 3-phosphate (Ga3P) position. Subsequent rapid metabolism produced intermediates characteristic of glycolysis and gluconeogenesis, such as glucose, phosphoenolpyruvate (PEP), pyruvate and lactate, among other metabolites[5]. Therefore, injection of hyperpolarized DHAc can provide insights on the reduction of DHAP to G3P (a pathway whose end point is the synthesis of new triglycerides in adipose cells) as well as on both directions of the glycolytic pathway (gluconeogenesis vs glycolysis).

The chemical shift range of the [2-^{13}C]DHAC and its metabolic products spans 144 ppm (over 4.6 kHz at 3T). To date, in vivo hyperpolarized ^{13}C-MR has mostly focused on limited portions of the ^{13}C-spectrum, corresponding to the chemical shift ranges of metabolites of key probes of interest such as [1-^{13}C]pyruvate to [1-^{13}C]lactate (which spans 24 ppm). For the optimal study of [2-^{13}C]DHAc MR acquisitions are required with broadband spectral coverage and accurate spatial localization to probe the distribution of its metabolic products in different organs. Currently, no general solution exists for the broadband spectral coverage required to investigate hyperpolarized [2-^{13}C]DHAc metabolism. A number of approaches have been attempted towards achieving adequate spectral coverage, mostly designed for [1-^{13}C]pyruvate studies.

In previous studies, narrow-band pulses were used to cover segments of the ^{13}C-spectrum in a series of excitations with multi-frequency shifts during RF transmissions[4,6]. Narrow-band pulses, however, are not suited for slice selection due to spatial misregistrations in the presence of chemical shift once the slice selection gradient is applied. Spectral-spatial (SPSP) RF pulses offer simultaneous control over frequencies, locations, and flip angles for hyperpolarized ^{13}C acquisitions[7,8,9]. However, previous pulses such as those optimized for the study of HP [1-^{13}C]pyruvate do not provide the 4.6-kHz-bandwidth required for the study of [2-^{13}C]DHAc metabolism at 3T. Outside the baseband of the SPSP pulse, aliased-bands can extend the spectral territory of SPSP several-fold, but typically include substantial spatial misregistrations. Fortunately, it is possible to exploit the typical sparsity of the ^{13}C spectrum for SPSP pulse design in the context of wide spectral separation, by targeting a few narrow frequency bands covering the distinct ^{13}C metabolite resonances. Challenges that stem from the broadband spectral coverage can be drastically reduced once constraints of sparse and narrow frequency bands are incorporated into the RF pulse design. Under these

assumptions, chemical-shift spatial misregistrations can then be corrected numerically under the small-tip approximation[10,11].

In addition to the issues mentioned above, the study of hyperpolarized [2-^{13}C]DHAc presents the typical technical challenges associated with in vivo hyperpolarized ^{13}C experiments. These include the sub-minute polarization decay constant and relatively low concentration of metabolic products. The hyperpolarized ^{13}C signal is normally lost within a minute or so, as polarizations of substrate and metabolic products rapidly decay to equilibrium level, which is governed by both the T_1 relaxation and chemical reactions. Furthermore, concentrations of metabolic products are generally much smaller than the injected hyperpolarized substrate. Therefore, improved SNR is achieved with larger flip angles for the metabolic products, while exciting the injected substrate with a lower flip angle[12]. This approach ensures that the magnetizations of both substrate and metabolic products can be detected in a more efficient and long-lasting manner.

In this work, we developed specialized SPSP pulse designs for MR investigations of hyperpolarized [2-^{13}C]DHAc that account for its wide spectral range by leveraging the sparse nature of the spectra to achieve the desired broadband excitation, while compensating for spatial misregistration effects and utilizing independent flip angle control over multiple frequency bands to improve detection SNR. In addition to the present application to hyperpolarized [2-^{13}C]DHAc, we envision that this approach will be applicable to other probes with similar spectral characteristics.

METHODS

Spectral-spatial RF pulse design considerations

The RF pulse was designed using an in-house developed software package in Matlab (The Mathworks Inc., Natick, MA). This software package is available online (http://www.radiology.ucsf.edu/research/labs/larson/software and https://github.com/agentmess/Spectral-Spatial-RF-Pulse-Design). Technical details of this software have been reported previously[12,13]. Briefly, it computes optimized RF and gradient pulses for a given spectral and spatial specification, including corrections for slice misregistration. The correction for misregistration has been extended in this study for broadband spectral coverage. Below are two central considerations for the design of this SPSP pulse.

First, because of the large spectral bandwidth, the spectral filter design must use the aliased copies of response to achieve the desired broadband specification with the low-bandwidth capabilities of SPSP pulses. This is achieved by designing a baseband spectral filter at a spectral sampling frequency, *Fs*, whose aliased copies at multiples of *Fs* meet the broadband specification. One key consideration is that all specified frequency bands, aliased or not, must be uniquely defined within the baseband filter such that the chemical shift misregistration correction can be performed (as described below). *Fs,* the inverse of the distance between the spatial subpulses, is chosen within the range [*Fmin, Fmax*]. The maximum sampling frequency, *Fmax*, is determined by the achievable maximal oscillating frequency of the gradient waveform, i.e. the inverse of the minimum-time gradient sublobe duration. The sublobe duration needs to satisfy the gradient amplitude and slew rate

constraints and spatial time-bandwidth (TBW). In this study, the oscillating gradient pulse was implemented using a symmetric echo-planar-imaging (EPI)-like waveform and the spatial TBW was set to be small (< 3), allowing a large *Fmax*. Meanwhile, the baseband should have enough width to accommodate the aliases of all frequency bands without causing overlaps of those aliased bands. This requires a sufficiently large sampling frequency, *Fmin*, which is the lower boundary of *Fs*. The SPSP pulse design software can determine the *Fs* within the range [*Fmin, Fmax*]. For each *Fs* that satisfies the aliased broadband specification, a baseband spectral filter is designed using convex optimization. These are combined with a spatial filter, designed based on the desired slice thickness, TBW, ripple, and phase response, to form an initial SPSP pulse design.

Second, the chemical shift slice misregistration is corrected for across all specified frequency bands. The slice misregistration is caused by the nonuniform sampling of the EPI gradient in excitation *kz-t* space, and this misregistration is more severe in a broadband SPSP pulse. A least-squares fit based on matrix pseudo-inversion was previously used to correct the slice misregistrations and shown to be effective for frequency bands designated in or around baseband[10,11]. However, the matrix pseudo-inversion has the tendency of amplifying coefficients of the spectral filter when the inversion problem is ill-conditioned. This is found in regions close to maximal or minimal *kz* where the EPI trajectory sampling is increasingly nonuniform. In this study, the least-squares pseudo-inversion was replaced by a regularized least-squares optimization that can be written as[14]

$$\underset{\beta_m}{argmin}\|W_{act}\beta_m - W_{ref}\beta_0\|_2+\lambda\|\beta_m\|_2 \quad \text{Eq. 1}$$

where W_{ref} is a Fourier operator on the targeted frequency bands, β_0 the uncorrected beta polynomial for the spectral filter, W_{act} a modified Fourier operator on the targeted frequency bands that includes the sample delays on the nonuniform sampling, β_m is the desired corrected beta polynomial for the spectral filter and λ a coefficient for regularization. The $\|\beta_m\|_2$ in Eq. 1 is a penalty on the total energy of spectral filter, which improves the stability or conditioning of the matrix inversion and also effectively keeps the peak power of the pulse from becoming too large. This regularized least-squares correction was performed for each *kz* line in the excitation *kz-t* space. In addition, the coefficient λ was empirically set to be 0.0001 in this study.

The RF pulse presented was designed to maximize the SNR from the metabolic products, while minimizing depolarization of the hyperpolarized substrate. Since DHAc and its hydrate are in equilibrium, keeping the small flip angle pulsed on both DHAc and DHAc-hydrate ensures minimal saturation of the substrate magnetization. The five-band SPSP RF pulse for a 1-cm slab described here is a 15.2 ms pulse with 0.276 G peak amplitude and *Fs* = 1420.5 Hz with a gradient amplitude of 43 mT/m and a maximum slew rate of 200 mT/m/ms (Figure 1a). The sample dwell time was 4 us for both gradient and RF.

The response of the RF pulse was specified for the following resonances and bandwidths at 3T: 213.0ppm ± 2ppm (DHAc) with 0.01% ripple, 151.0ppm ± 1ppm (PEP) with 0.04% ripple, 96.1ppm ± 1ppm (DHAc hydrate) with 0.04% ripple, 88.0ppm ± 1ppm (additional

frequency band) with 0.04% ripple, and 73.0ppm ± 3ppm (G3P) with 0.04% ripple. The RF pulse was designed for a 0° flip on DHAc; a 67.5° flip angle on PEP; a 4.5° flip on DHAc hydrate; and a 45° flip on G3P and 88.0 ppm bands. A minimum-phase spectral filter was used to reduce the pulse duration and peak power. The simulated spectral performance of the pulse at the center of the slab and the spatial excitation profile for the controlled frequency bands can be seen in Figure 1b and c, respectively. The solid black curve corresponds to the profiles of the SPSP RF pulse used in this study, evidencing the lack of chemical shift misregistration errors for the pulse across the large bandwidth. In contrast, the dashed red curve displays the misregistration effects when no phase correction is performed.

To demonstrate the flexibility of this SPSP RF design approach, a six-band SPSP RF pulse for 2-cm slabs was created similarly as above with an additional band at 180.8 ppm and slightly different center frequencies for each band (Supporting Figure S1).

Spectral-spatial RF pulse performance in a ^{13}C-urea phantom

The performance of the five- and six-band RF pulse was tested using three 1-ml vials filled with thermally polarized ^{13}C-enriched urea (6.0 M) in a 3T clinical MRI system (GE Healthcare, Waukesha, WI, USA) equipped with 50 mT/m, 200 mT/m/ms gradients and a broadband RF amplifier. ^{1}H and ^{13}C RF transmission and signal reception was performed with a custom-built, dual-tuned rat birdcage coil. Since ^{13}C-urea presents a single resonance, the transmitter offset was shifted to get representative data of the behavior of the pulse at the specified frequency bands.

The RF pulse peak power and gradient hardware delay were calibrated manually to produce (a) a 29° flip at the transmitter offset −2928 Hz for the six-bands SPSP pulse, and (b) a 20° flip at the transmitter offset −2895 Hz for the five-bands SPSP pulse. These transmitter offset frequencies correspond to the G3P resonance targeted with each pulse design. Signals were recorded after exciting a 2-cm slab centered on slices above, below and through the phantom at the transmitter offsets corresponding to the center offset frequency of each band (Figure 3a). Several gradient delay times, t_{del}, were tested and measurements were performed with the optimal delay (t_{del} =−4 us).

Sample preparation and hyperpolarization

A stock solution was prepared with 500 mg [2-^{13}C]DHAc-dimer (99% ^{13}C, Sigma Aldrich, Miamisburg, OH; ~8 M final concentration of [2-^{13}C]DHAc), 343 ul of 2:1 water:DMSO (vol/vol), 21 mg of trityl radical OX063 (Oxford Instruments, Abingdon, UK; ~21mM final concentration) and 1.38 ul 500 mM gadolinium-DOTA chelate (Guerbet, Roissy, France; ~1.0 mM final concentration). A 40ul aliquot of this solution was polarized at 3.35 T and 1.3 K using an Oxford HyperSense instrument (Abingdon, U.K.). The sample was irradiated for 1.5 hours with 20 mW microwaves at 94.095 GHz. The material was then dissolved in 4 ml of a superheated solution of phosphate buffered saline (neutral pH) to obtain a final concentration of ~80 mM of [2-^{13}C]DHAc. In solution, the polarization level of [2-^{13}C]DHAc was ~8% 20 s after dissolution.

Animal preparation

All animal studies were carried out under a protocol approved by the University of California San Francisco (UCSF) Institutional Animal Care and Use Committee.

Nine Sprague Dawley rats (age = 3-5 months, weight = 0.45-0.5 kg) were fasted for 24 hours and anesthetized prior to the MRS experiments by administration of inhalational isofluorane via nose cone (2.5%, 1 l/min). A tail-vein cannula was inserted for hyperpolarized agent administration, and its patency maintained with heparin diluted in sterile saline (4 U/ml). The animal was placed on a warm pad inside the dual-tuned birdcage coil to maintain its body temperature at 37°C and isofluorane delivery was kept at 1.5-1.7% (1 l/min) throughout the experiment.

MR spectroscopy in vivo

In vivo experiments were performed using the 3T clinical MRI system and birdcage coil described above. ^{1}H images were acquired for anatomic reference. ^{13}C power and center frequency calibration were performed using a 1 ml vial filled with 6.0 M ^{13}C-urea placed next to the rat kidney in the coil.

Two different methods for spatial-spectral localization of the metabolic resonances were employed: (a) multi-frequency shifts, where the RF frequency offset was moved sequentially to excite a region of interest every second and required multiple acquisitions, and (b) multi-band SPSP RF pulse, where the whole spectrum was acquired in one acquisition. In both cases, 2.5 ml of hyperpolarized [2-^{13}C]DHAc solution was injected into the tail vein of a rat over 12 s and MRS acquisition started 15 s after the beginning of the injection. A schematic diagram on how each method was applied is shown in Figure 2.

Multi-frequency shifts—In order to localize the excitation to a 2-cm thick axial slab on either the liver or the kidney, a 694.4 Hz-band spatially-selective Gaussian RF pulse was used. The RF offset was moved to center the excitation band on different resonances alternately and the flip angle was also changed for each band: 5° on the region of DHAc resonance (213 ppm), 20° at 180 ppm (additional resonance), 30° at 150 ppm (PEP resonance), 20° at 89 ppm (additional resonance), and 20° at 69 ppm (G3P resonance).

As shown in the diagram in Figure 2 (top), there was a 1 s temporal delay between acquisition of each band. For dynamic spectral acquisition, the same band was excited every 5 s. A 2-cm axial slab centered on the liver was excited, followed by the excitation of 2-cm axial slab centered on a kidney 0.5 s later (inter-slab separation=1.7 cm).

Multi-band SPSP RF pulse and 2D MR Spectroscopic Imaging—Axial slabs of 1 cm thickness were excited on either the liver or the kidney with the five-band SPSP RF pulse centered on the urea phantom resonance at 163.2 ppm, with a temporal delay of 1.5 s between the liver and kidney acquisitions (Figure 2, bottom). Additional acquisition parameters included: TR for dynamic acquisition = 3 s; receiver bandwidth = 10 kHz; number of points = 2048; flip angle = 0.3° at the DHAc resonance (213 ppm), 26° at the PEP resonance (151 ppm), 2.3° at the DHAc hydrate resonance (96 ppm), 20° at an additional resonance at 88 ppm, and 20° at the G3P resonance (73 ppm). The relative

metabolite concentrations within each slab were quantified by integrating the area under the peaks of interest and normalizing them against the integral of the first DHAc hydrate peak within the same slab.

To demonstrate the potential of the SPSP pulses presented here, a 2D MRSI image with compressed sensing acceleration was acquired from an axial slab across the liver excited using the five-band SPSP RF pulse. The 2D MRSI was performed with random walk k-space trajectories, 3.8-fold undersampling scheme and compressed sensing reconstruction. In this sequence, gradient blips with random amplitudes and intervals were added during the readout period, allowing readout along multiple random walk trajectories in *kx-ky-t*-space. Previous work has described gradient blips with random amplitudes [15–17], which was extended to have random time intervals for this work to support a large spectral bandwidth. The 3.8-fold undersampling scheme consisted 14 phase encodings in each image frame. Among them, 10 phase encodings performed the above-mentioned random walks in *kx-ky-t*-space. The other 4 phase encodings fully sampled the time dimension of center *kx-ky*-space. The other acquisition parameters were: TE/TR = 10/150 ms, slab thickness = 2 cm, 2D matrix = 8 × 8, FOV = 8 × 8 cm^2, spectral bandwidth = 10 KHz, 14 excitations for one image frame, 20 dynamic frames, temporal resolution = 3 second/frame, acquisition started 15 s after the beginning of the substrate injection. Lastly, the CS reconstruction was performing by L_1-minimization, exploring the spatial and spectral sparsity[18]. A detailed description of the sampling pattern and the reconstruction will be provided in a separate study.

RESULTS

SPSP RF pulse performance in a ^{13}C-urea phantom

Signals arising from the excitation of 2-cm slabs centered on slices above, below and through a ^{13}C-urea phantom (Figure 3a) were measured and compared to the simulated signals. Figure 3b and c display the performance of the six-band and five-band SPSP RF pulses, respectively.

The signal intensity measured at each frequency on the slab centered in the phantom agreed with the expected signal calculated by simulations of both SPSP pulses. Across the spatial-spectrally selected frequencies for excitation, the maximum discrepancy from the simulations was found at the largest flip angle, with a difference of 6% at −424 Hz for six-band SPSP (~39° flip), and a difference of 5% at −392 Hz for five-band SPSP (~26° flip).

Spatial selectivity was assessed by comparing the signals from a slab through the phantom with slabs above and below the phantom. For the six-band SPSP pulse, higher signal intensity was measured from the slab centered across the phantom than from the slabs centered outside by approximately 12-fold at 565 Hz (additional resonance), 39-fold at −424 Hz (PEP resonance), 23-fold at −2414 Hz (additional resonance), and 95-fold at −2928 Hz (G3P resonance). At 1599 Hz (DHAc resonance) and −2157 Hz (DHAc hydrate resonance), where spatial selection was not controlled by this pulse, the signal intensity inside the phantom was about 10-fold smaller and 3-fold larger than the signal outside the phantom, respectively.

Similarly, for the five-band SPSP pulse, the slab centered across the phantom gave more signal than the slabs centered outside by about 47x at −392 Hz (PEP resonance), 4x at −2154 Hz (DHAc hydrate resonance), 34x at −2414 Hz (additional resonance), and 35x at −2895 Hz (G3P resonance). Note that the small difference between the signal from a slab centered inside and outside the phantom at the transmitter offset corresponding to DHAc hydrate (−2154 Hz) is only 4x because the flip angle applied is about 2°, while the other resonances are excited with flip angles over 20°. At 1599 Hz (DHAc resonance) spatial selection was not controlled.

In vivo MRS using multi-frequency shifts

Figure 4 shows representative ^{13}C-spectra from a liver slab (black curve) and a kidney slab (red curve) from a fasted rat upon injection of [2-^{13}C]DHAc and acquired using the multi-frequency shifts method. Signal within the excitation bandwidth on each spectrum (shaded) arises from the selected slab, either liver or kidney. Signal from outside the shaded area, however, was the result of spatial misregistration and belonged to a different slab. With the slice thickness and excitation RF pulse used here, a peak found 20 ppm (642 Hz) away from the center of the excitation band, for instance, originated from 1.8 cm above or below the center of the prescribed slab.

After adding the first five spectra with the same RF center frequency, and before normalization of the data, the approximate SNR of the resonances of interest in the liver were 1177 for DHAc, 45 for PEP, 1118 for DHAc hydrate and 46 for G3P. In the kidneys, the SNRs were 2312 for DHAc, 14 for PEP, 1137 for DHAc hydrate, and 30 for G3P.

In vivo MRS using the multi-band spectral-spatial RF pulse

The multi-band SPSP RF pulse allowed for simultaneous acquisition of all the resonances of interest within the selected slab.

^{13}C-spectra were acquired on the same rat and the same slabs prescribed above upon injection of hyperpolarized [2-^{13}C]DHAc using the six-bands SPSP RF pulse (Supporting Figure S2a). The SNR of the sum of the first five spectra within the liver slab for the PEP resonance was 32 and that of the G3P was 281. In the kidney slab, the SNRs were 25 and 81 for PEP and G3P, respectively. DHAc and its hydrate were not spatially controlled, and therefore were not quantitative. Urea signal originating from phantom could be seen on the kidney slab because it was deliberately placed on top of the kidney as a control. As expected, no urea signal was observed in the liver slab.

Hyperpolarized [2-^{13}C]DHAc ^{13}C-spectra were also acquired using the five-band SPSP RF pulse on five fasted rats. Representatively in one of the experiments, the SNR of the sum of the first five spectra within the liver slab for the PEP resonance was 34, 107 for that of the G3P, and 200 for the DHAc hydrate resonance. In the kidney slab, the SNRs were 32, 73 and 1341 for PEP, G3P and DHAc hydrate, respectively. Figure 5a shows an example of the ^{13}C-spectra obtained from the liver slabs (black curve) and the kidney slabs (red curve). Spectra were normalized to the integral of the DHAc-hydrate signal (DHAc was not spatially controlled, and thus not suitable for normalization). Dynamic ^{13}C-MRS SNR data for the first 100 s from the metabolic products of DHAc from liver and kidney are shown in Figure

5b top and bottom, respectively. The bar plot in Figure 5c displays the mean liver over kidney ratio of PEP and G3P upon summing the integrals of the first five time points for each metabolite. There was ~4x more PEP in the liver than in the kidney, and ~19x more G3P. Results for each individual rat are displayed in Table 1.

Using the same SPSP RF pulse, the spectra of a syringe filled with hyperpolarized [2-^{13}C]DHAc solution was acquired and impurities of the injected substrate were detected in resonances not overlaying with the metabolic products of DHAc (Supporting Figure S2b). These impurities can also be seen in Figure 5a. The T_1 of [2-^{13}C]DHAc was measured to be ~40 s in solution and ~25 s in vivo at 3T.

Figure 6 is a representative 2D MRSI from a dynamic acquisition of an axial slab across the liver upon injection of [2-^{13}C]DHAc. The liver contour has been loosely highlighted with a yellow curve. Production of G3P is detected within the liver, while little to no G3P is observed outside the organ.

DISCUSSION

Development of a five-band SPSP RF pulse with excitation over a 4.6-KHz bandwidth

This study developed and applied a new SPSP RF pulse for probing [2-^{13}C]DHAc and its metabolic products, with an excitation profile over 144 ppm at 3T (4.6 kHz). The SPSP RF pulse was developed with constraints over five and six sparsely distributed frequency bands in the ^{13}C-spectrum, optimized on conditions of minimizing flip angle at DHAc and DHAc hydrate while delivering a higher flip angle to the metabolites, and correcting for chemical shift slice misregistration across all bands. This is the first broadband SPSP design, to our knowledge, with five frequency bands for excitation over a 4.6-kHz bandwidth. In vivo experiments were performed on rat liver and kidney under fasting conditions, demonstrating the SPSP RF pulse capability to investigate [2-^{13}C]DHAc metabolism in different organs in vivo. The 15 ms duration of the SPSP RF pulse is not an issue for ^{13}C-metabolites, which have T_2 relaxation time constants larger than 100 ms [19,20]. Also, approximate T_2* values of ^{13}C metabolites in our 3T scanner are typically ~50 ms, which is still relatively long as compared to our pulse duration.

Tests on ^{13}C-phantom solutions showed that the multi-band SPSP RF pulses provided the desired tailored excitation, meeting requirements for both spatial and spectral selectivity. In our experience, the 3T clinical scanner used for these experiments has an efficient in-built eddy-current compensation that minimizes eddy-current induced field distortions, even when using the scanner at maximum gradient performance. A maximum difference of 6% between the measured and calculated RF pulse profile inside the phantom was measured for the largest flip angle (~39° at −424 Hz on the 6-band SPSP RF pulse). However, these SPSP RF pulses are sensitive to how accurately the waveforms are played out by the scanner hardware, and gradient eddy currents could be a problem, because of the symmetric EPI-like gradient. To address this, a simplistic correction factor, *tdel,* was applied to shift the relative timing of the RF and gradient waveforms in this study. While this approach appeared to be adequate in these studies, more sophisticated corrections could be incorporated into the pulse design to eliminate unexpected pulse behavior, such as actual measurements of the

gradient and RF waveforms (the RF amplifier bandwidth may also distort the pulse profile due to large frequency separation of the bands in the pulse).

Like most SPSP pulses, the narrow excitation bands can be sensitive to frequency drifts, and accurate knowledge of the resonances in vivo is required for the pulse design. In this study, each band was designed with at least a ± 1ppm bandwidth, and resonances were determined from initial tests with non-selective broadband excitations and the multi-frequency shifts spectra.

Hyperpolarized [2-^{13}C]DHAc in rat liver and kidney in vivo

Comparing in vivo data acquired with both methods, spectra with higher SNR were obtained with the SPSP RF pulse. This method also made it possible to acquire all the resonances of interest simultaneously without chemical shift misregistration. Therefore, spectral acquisition could be started during injection of the hyperpolarized agent without fear of saturating DHAc on other slabs due to misregistration during delivery. On average we observed a shift of ~27 Hz (0.84 ppm at 3T) between liver and kidneys. The excitation bands of the SPSP RF pulse are designed to cover efficiently a range of at least ± 32.1 Hz (± 1 ppm) around the defined center frequency of the band. In our experience, deviation of the observed peaks from the chosen center frequency does not exceed 32.1 Hz. Derived from the simulation in Figure 2c, the flip angle varies a maximum 7% across the excitation band corresponding to the PEP resonance (i.e. from 26° to 24°) and 11% across the G3P resonance (from 20° to 18°). At the edges of the DHAc hydrate resonance, the flip angle drops by 22%, but since the expected excitation angle is very small, the effect is negligible (i.e. from 2° to 1.8°).

The multi-frequency shifts method allows for visualization of the metabolites in the different slabs, but quantification is not reliable due to the following reasons: frequency bands are not acquired simultaneously, and unintentional excitation of the substrate in a different slab leads to broad baseline that can mask or incorrectly boost the integral of small peaks, such as PEP. Although a single-band spectral-spatial pulse could be designed for use in the multi-frequency shifts method (with attention given to aliases to guarantee that no other metabolic resonances are excited), the issue of simultaneous acquisition of all the metabolites would remain unaddressed.

The ^{13}C-spectra obtained with the five-band SPSP RF pulse acquisition in vivo produced a high-SNR G3P peak, clearly indicating that there was 19 times more G3P in the liver than in the kidney. This in not a surprising result, since liver is the main regulator of triglycerides production. PEP was also observable, albeit with lower SNR. A 1cm-slab allows for clear separation between liver and kidneys in a rat of ~0.5 kg (Figure 5d), and since within this slab gluconeogenesis and glycolysis are performed mainly in these organs, one can reasonably assume that the metabolic products of DHAc observed on the spectra are mostly generated in this organs and not very substantially produced in vasculature or other organs partially captured in the slab (i.e. stomach).

This study has also demonstrated the potential of these SPSP RF pulses to perform MRS imaging. Here, a 2D MRS image localizing the G3P production within the liver has been

displayed, and it could be extended to 3D MRS imaging for multi-slice acquisition. This feature would allow spatial localization of the metabolic signal from within small voxels, while preserving the spectral selectivity of the resonances of interest. The ratios between the SNR of spectra acquired from a 1cm-slab across the liver spectrum (Figure 5b) and the SNR of spectra from a liver voxel from the 2D MRSI (Figure 6c) are 1.6-2.4 for G3P and 1.5-3 for DHAc hydrate. From the MRSI image, the G3P signal arises mainly from ~12 voxels. If one assumes that the G3P signal on the slice-selective spectra comes from the same area, a signal difference of ~2.4 is expected. The discrepancy between the calculated result and the ratios measured arises from the fact that in a slab, the signal contribution from vasculature and other organs gets diluted by the high signal produced by the liver, while a vessel may be the main source of signal in a smaller voxel.

CONCLUSIONS

A new spectral-spatial pulse design was developed and applied to acquire ^{13}C-spectra of hyperpolarized [2-^{13}C]DHAc, a new marker of gluconeogenesis in the rat liver and kidney in vivo. The metabolic products PEP and G3P were detected, evidencing metabolism of the hyperpolarized substrate in the glycolytic pathway and activity of the enzyme glycerol 3-phosphate dehydrogenase.

Since the resonances originated from the metabolism of [2-^{13}C]DHAc range over 144 ppm (69-213ppm, 4.6 KHz at 3T), a novel excitation and acquisition method was required. We developed a spatially selective multi-band SPSP RF pulse that allows for simultaneous excitation with independent flip angle control at five or six frequency bands over a 4.6 KHz frequency range. A key feature of these pulses is that chemical shift misregistration is corrected for, resulting in accurate spatial-spectral selectivity across the bands of interest. In addition, the SPSP design is flexible and the spectral profile could be readily modified to study other metabolites with large chemical shift differences, e.g. [2-^{13}C]pyruvate and its products.

Supplementary Material

Refer to Web version on PubMed Central for supplementary material.

ACKNOWLEDGEMENTS

We thank Dr. Robert Bok for experimental help. This work was supported by an intramural UCSF radiology department seed grant, and NIH grants P41EB013598, P41EB015908, R21EB016197, R01EB016741, and R37HL34557. CVM was supported by NIH K01DK099451.

REFERENCES

1. Brindle KM. Imaging metabolism with hyperpolarized 13C-labeled cell substrates. J Am Chem Soc. 2015; 137:6418–6427. [PubMed: 25950268]
2. Chaumeil MM, Najac C, Ronen SM. Studies of metabolism using 13C MRS of hyperpolarized probes. Methods Enzymol. 2015; 561:1–71. [PubMed: 26358901]
3. Albers MJ, Bok R, Chen AP, Cunningham CH, Zierhut ML, Zhang VY, Kohler SJ, Tropp J, Hurd RE, Yen YF, et al. Hyperpolarized 13C lactate, pyruvate, and alanine: noninvasive biomarkers for prostate cancer detection and grading. Cancer Res. 2008; 68(20):8607–8615. [PubMed: 18922937]

4. Lau AZ, Chen AP, Ghugre NR, Ramanan V, Lam WW, Connelly K a, Wright G a, Cunningham CH. Rapid multislice imaging of hyperpolarized 13C pyruvate and bicarbonate in the heart. Magn Reson Med. 2010; 64(5):1323–31. [PubMed: 20574989]
5. Moreno KX, Satapati S, DeBerardinis RJ, Burgess SC, Malloy CR, Merritt ME. Real-time detection of hepatic gluconeogenic and glycogenolytic states using hyperpolarized [2-13C]dihydroxyacetone. J Biol Chem. 2014; 289:35859–35867. [PubMed: 25352600]
6. Josan S, Hurd R, Park JM, Yen Y-F, Watkins R, Pfefferbaum A, Spielman D, Mayer D. Dynamic metabolic imaging of hyperpolarized [2-13C]pyruvate using spiral CSI with alternating spectral band excitation. Magn Reson Med. 2014; 71(6):2051–2058. [PubMed: 23878057]
7. Chen WC, Teo XQ, Lee MY, Radda GK, Lee P. Robust hyperpolarized 13C metabolic imaging with selective non-excitation of pyruvate (SNEP). NMR Biomed. 2015; 28(8):1021–1030. [PubMed: 26119950]
8. Harris T, Degani H, Frydman L. Hyperpolarized 13C NMR studies of glucose metabolism in living breast cancer cell cultures. NMR Biomed. 2013; 26(12):1831–1843. [PubMed: 24115045]
9. Lau AZ, Chen AP, Hurd RE, Cunningham CH. Spectral-spatial excitation for rapid imaging of DNP compounds. NMR Biomed. 2011; 24(8):988–96. [PubMed: 21751271]
10. Cunningham, C., Chen, A., Vigneron, D., Lustig, M., Kelley, D., Xu, D., Pauly, J. Proc Intl Soc Mag Reson Med. Vol. Vol. 14. Seattle: 2006. Spectral-spatial excitation and refocusing for reduced volume mis-registration at 7 Tesla; p. 72
11. Cunningham CH, Chen AP, Lustig M, Lupo J, Xu D, Hurd RE, Pauly JM, Nelson SJ, Vigneron DB. Pulse sequence for dynamic volumetric imaging of hyperpolarized metabolic products. J Magn Reson. 2008; 193(1):139–146. [PubMed: 18424203]
12. Larson PEZ, Kerr AB, Chen AP, Lustig M, Zierhut ML, Hu S, Cunningham CH, Pauly JM, Kurhanewicz J, Vigneron DB. Multiband excitation pulses for hyperpolarized 13C dynamic chemical shift imaging. J Magn Reson. 2008; 194(1):121–127. [PubMed: 18619875]
13. Kerr, AB., Larson, P., Lustig, M., Cunningham, CH., Chen, AP., Vigneron, DB., Pauly, JM. Proc Intl Soc Mag Reson Med. Vol. Vol. 16. Toronto: 2008. Multiband spectral-spatial design for high-field and hyperpolarized C-13 applications; p. 226
14. Press, WH., Teukolsky, SA., Vetterling, WT., Flannery, BP. Numerical Recipes 3rd Edition: The Art of Scientific Computing. 3rd ed. Cambridge University Press; New York, NY, USA: 2007.
15. Hu S, Lustig M, Chen AP, Crane J, Kerr A, Douglas AC, Hurd R, Kurhanewicz J, Nelson SJ, Pauly JM, et al. Compressed sensing for resolution enhancement of hyperpolarized 13C flyback 3D-MRSI. 2008; 192(2):258–264.
16. Hu S, Lustig M, Balakrishnan A. 3D compressed sensing for highly accelerated hyperpolarized 13C MRSI with in vivo applications to transgenic mouse models of cancer. Magn Reson Med. 2010; 63(2):312–321. [PubMed: 20017160]
17. Larson PEZ, Hu S, Lustig M, Kerr AB, Nelson SJ, Kurhanewicz J, Pauly JM, Vigneron DB. Fast dynamic 3D MRSI with compressed sensing and multiband excitation pulses for hyperpolarized 13C studies. Magn Reson Med. 2011; 65(3):610–619. [PubMed: 20939089]
18. Lustig M, Donoho DL, Pauly JM. Sparse MRI: The application of compressed sensing for rapid MR imaging. Magn Reson Med. 2007; 58(6):1182–1195. [PubMed: 17969013]
19. Reed GD, von Morze C, Bok R, Koelsch BL, Van Criekinge M, Smith KJ, Hong Shang, Larson PEZ, Kurhanewicz J, Vigneron DB. High resolution 13C MRI with hyperpolarized urea: in vivo T2 mapping and 15N labeling effects. 2014; 33(2):362–371.
20. Yen YF, Roux P Le, Mayer D, King R, Spielman D, Tropp J, Pauly KB, Pfefferbaum A, Vasanawala S, Hurd R. T2 relaxation times of 13C metabolites in a rat hepatocellular carcinoma model measured in vivo using 13C-MRS of hyperpolarized [1-13C]pyruvate. NMR in Biomedicine. May.2010 23:414–423. 2009. [PubMed: 20175135]

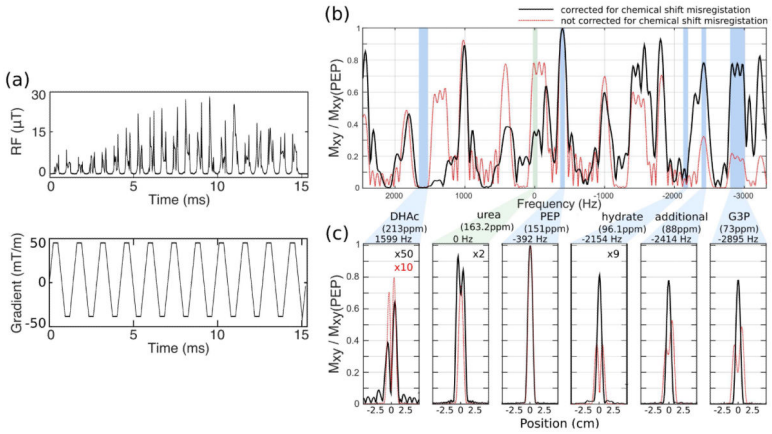

Figure 1.

Spectral-spatial RF excitation pulse with independent flip angle control over five excitation bands. (a) RF and gradient waveforms. This 15.2 ms pulse was designed for a 1-cm slab, with the following resonances and their corresponding bandwidths and flip angles: 213.0ppm ± 2ppm (DHAc), 0°; 151.0ppm ± 1ppm (PEP), 67.5°; 96.1ppm ± 1ppm (DHAc hydrate), 0°; 88.0ppm ± 1ppm (additional resonance), 45°; and 73.0ppm ± 3ppm (G3P), 45°. (b) Spectral profile at the center of the slab (at 0 cm) and (b) spatial profile. The black curve displays the profiles of the RF designed with chemical shift misregistration correction (RF pulse shown in (a)), while the red curve characterizes the profiles. Urea was chosen as the center offset (0 Hz) envisioning the use of a urea phantom as a reference during in vivo experiments. Urea was not, however, one of the frequency bands controlled during the design of the experiment, which lead to a broader slice profile.

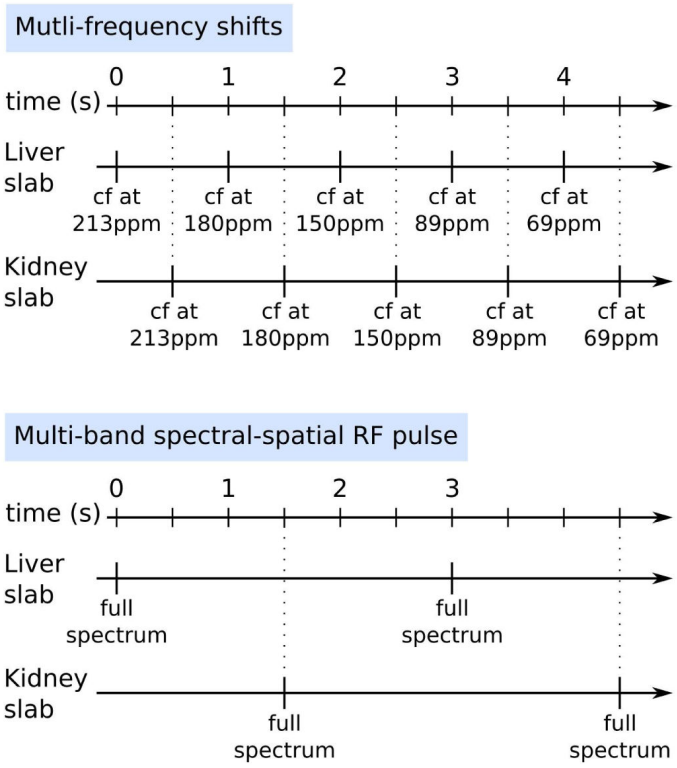

Figure 2.

Schema of the two methods used for the acquisition of the [2-^{13}C]DHAc spectra. For the "Multi-frequency shifts" method, the RF offset was changed to center a 21.6ppm effective excitation band for the spatially-selective pulses used on the metabolite region of interest, although slice misregistration resulted in excitation out of this band. The TR between excitations on the same band was 5 s. Conversely, the SPSP RF pulse allowed for acquisition of all the resonances of interest in a single excitation with no slice misregistration, and a TR of 3 s was chosen for dynamic spectra acquisition. Liver and kidney acquisitions were interleaved in both methods.

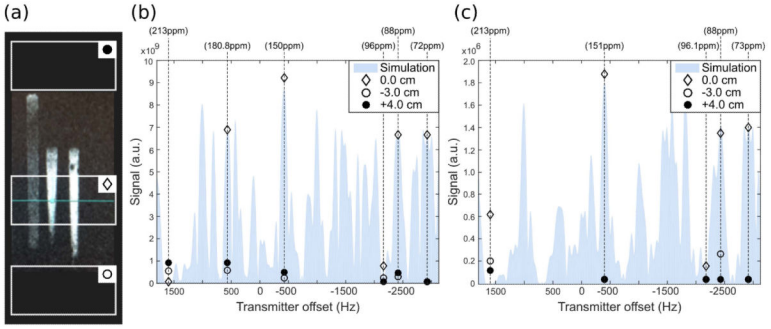

Figure 3.

Signal intensity measurements of the SPSP RF pulse performance on slabs above, below, and through a ^{13}C-urea phantom. (a) Sketch of the 2-cm-slab positions on the three syringes filled with a ^{13}C-urea solution used as a phantom. (b) Six-band SPSP RF pulse performance. RF flip = 29° was calibrated at the transmitter frequency −2928 Hz (*tdel*=−4 us). (c) Five-band SPSP RF pulse performance. RF flip = 20° calibrated at the transmitter frequency −2895 Hz (*tdel*=−4 us). These calibration frequencies correspond to the G3P resonance as targeted in each pulse design. Shaded area is the simulated signal in the slab through the phantom.

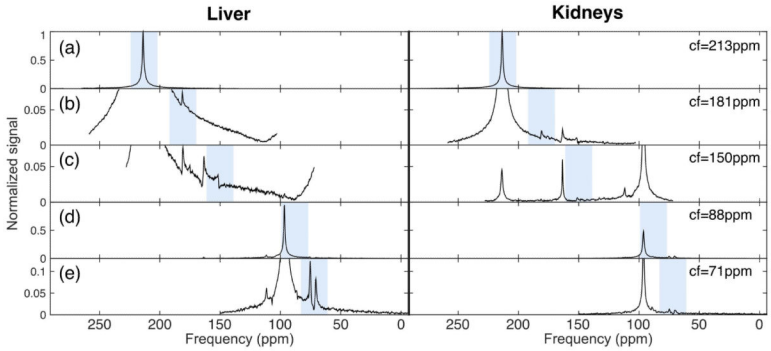

Figure 4.

^{13}C-MRS acquired using the multi-frequency shifts method on a 2-cm slab on the liver and a 2-cm slab on the kidney. The RF pulse excitation bandwidth was 694.4 Hz (21.6ppm), whilst the acquisition bandwidth was 5 KHz (155.8ppm), centered on the frequency offset specified on the right of the image. The shaded areas highlight the excitation band on the center of the prescribed slab. Misregistered resonances can be seen outside the shaded area. The following flip angles were applied on each band: (a) 5°, (b,d,e) 20°, and (c) 30°. Signal was normalized to the DHAc peak in (a). Data shown is the sum of the first five dynamic spectra.

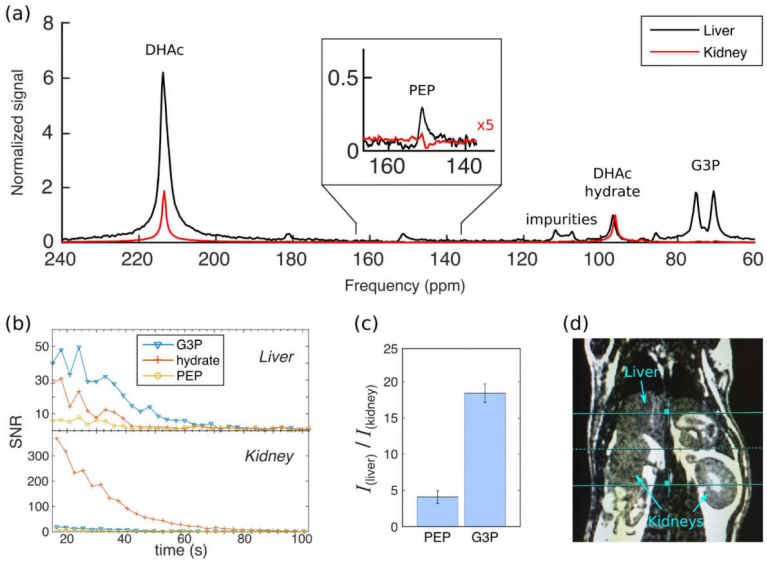

Figure 5.

(a) ^{13}C-MRS upon injection of hyperpolarized [2-^{13}C]DHAc into a fasted rat using a five-band SPSP RF pulse to excite a 1-cm slab placed on the liver (black) and a 1-cm slab placed on the kidney (red). The following flip angles were applied: 0.3° at 213 ppm, 26° at 151 ppm, 2.3° at 96 ppm, 20° at 88 ppm and 20° at 73 ppm. The spectrum shown is the sum of the first five acquisitions. (b) Dynamic curves of the SNR of the metabolic products from (a). (c) Ratio of the integrals of the first five time points of PEP and G3P from the liver over the kidney (mean ± std, n=9). (d) Anatomic reference of the liver and kidney slabs.

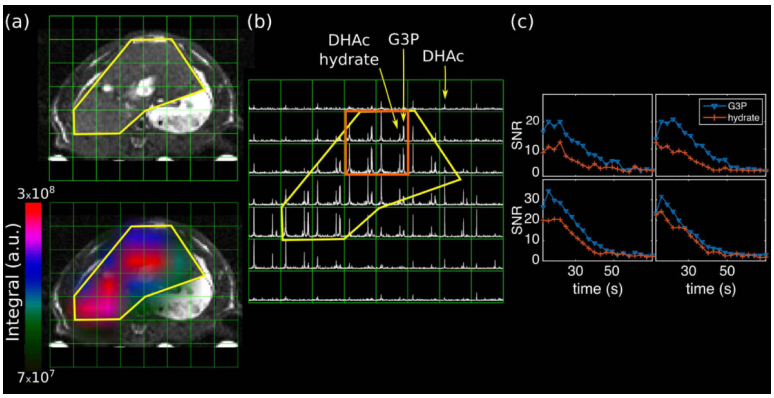

Figure 6.

Axial 2D MRSI of the liver. (a) A 3D balanced-SSFP ^{1}H image is shown for anatomic reference, and on the bottom is the same image with the G3P metabolite map overlayed on it. The liver contour is delineated in yellow, highlighting that metabolism of DHAc occurs mainly inside this organ. (b) Axial 2D ^{13}C-MRSI acquired 12 s after the start of the injection of hyperpolarized [2-^{13}C]DHAc into a fasted rat using the same SPSP RF pulse as in Figure 5. Acquisition parameters: slab thickness = 2 cm, matrix = 8 × 8, FOV = 8 × 8 cm^2, 10° flip angle calibrated at the transmitter frequency offset −2895 Hz. (c) Dynamic curves of the SNR of G3P and DHAc hydrate from the four voxels highlighted in orange.

Table 1

Integrated hyperpolarized DHAc metabolite ratios (liver over kidney). Data were normalized to the DHAc hydrate integral of each organ prior to ratio calculation. The mean result is shown also in **Figure 5**c.

	PEP (liver/kidney)	G3P (liver/kidney)
Rat #1	3.4	18.2
Rat #2	4.3	17.9
Rat #3	2.3	20.9
Rat #4	3.7	19.5
Rat #5	3.6	18.7
Rat #6	4.1	17.4
Rat #7	5.4	19.0
Rat #8	4.7	19.0
Rat #9	4.7	19.8
Mean	4.1 ± 0.9	18.7 ± 1.3